

Dynamic Analysis of Geosynthetic-reinforced Pile-supported Embankment for a High-Speed Rail

Rashad Alsirawan, Edina Koch

Széchenyi István University. Egyetem tér 1, H-9026 Győr, Hungary
alsirawan.rashad@sze.hu, koche@sze.hu

Abstract: Geosynthetic-Reinforced-Pile-Supported (GRPS) embankments are a trustworthy option ideal to support the railways over soft soils. They are widely used for the time-bound infrastructure projects. The majority of earlier research concentrated on the analysis of the GRPS embankments under static loads while the studies on the behavior of these constructions under dynamic loads are scarce. The fundamental purpose of this study has been to better comprehend the dynamic behavior of GRPS embankments in terms of stresses and settlements distribution via 3D modeling employing the finite element method (FEM). The advanced constitutive model of Hardening soil with small-strain stiffness was utilized to simulate the behavior of the soils under dynamic loads and the train load was modeled according to the recommendations of LM71 Eurocode. The results indicate to the contribution of the piles and geosynthetic reinforcement in the decrease of the settlements. The behavior of settlements and stresses under static and dynamic loads is similar. The load efficiency of the piles decreases during the passage of the train remarkably. The train speed affects obviously on the behavior of the GRPS embankment

Keywords: GRPS embankment; 3D modeling; stresses and settlements distribution; dynamic loads; load efficiency

1 Introduction

Rail transport is among the most ecologically responsible solutions of transportation in the world since it relies heavily on electric haulage [1]. Generally, the geosynthetic reinforcement with piles is considered an ideal solution to support the embankments of high-speed railways over soft soil layers [2]. This technology contributes to substantially reduce embankment settlement, construction time, and cost [3].

The behavior of Geosynthetic-Reinforced Pile-Supported (GRPS) embankments under static loading is investigated extensively. The mechanism of load transfer in the GRPS embankments is described as a combination of different phenomena:

the soil arching due to the difference between stiffness of piles and surrounding soft soil, tensioned membrane effect of the geosynthetic, frictional behavior of soil-geosynthetic interface and the soft soil support. Different researchers have investigated the behavior of GRPS embankments and suggested many analytical methods of design (Terzaghi [4], Low *et al.* [5], Russell & Pierpoint [6], Abusharar *et al.* [7], BS 8006 [8], EBGEO [9], CUR226 [10], Pham [11]).

In regards of cyclic loading, the literature review is much more limited, however the behavior of the GRPS embankment under this type of loading is crucial owing to the real representation of the problem. Heitz *et al.* [12] indicated that numerous factors reduce the soil arching and, as a result, the load efficiency (E is the ratio of load applied over the pile head to the total load). Based on a small-scale model of a GRPS embankment exposed to cyclic loading. These factors include pile configuration, layers of geosynthetic, number of cycles, and loading frequency. Yu *et al.* [13] compared the difference in the behavior of piled embankment under static and traffic loads, the results indicate that the soil arching phenomenon has disappeared after 300 cycles and the vertical stress carried by the soft soil increases with the cycle numbers. Han and Bhandari [14] developed a 2D discrete element model (DEM) of a GRPS embankment and discovered that the stress concentration ratio (SCR is the ratio of the stress over the pile head to the stress over the soft soil in a unit cell) and the geogrid tension increase as the embankment height, geogrid stiffness, and pile elastic modulus increase under cyclic loads.

Han *et al.* [15] created a laboratory model and the model tests was followed by FE analysis. The findings indicate that the dynamic load has an obvious influence on the soil arching if the embankment height is not enough. Moreover, the geogrid presence contributes in more stability of the soil arch if the ratio of embankment height to pile spacing is more than 1.4. Zhuang *et al.* [16] investigated the behavior of piled embankment using FE method and Mohr–Coulomb to model the embankment soil. The results indicated that the applied vertical stress over the pile cap increases with the increase of cyclic loading to a certain point of time and then decreases due to the reduction of the soil arching. The vertical stress increases also with the decrease of the vehicle speed. The researchers stated that the complicated dynamic soil behavior of the embankment cannot be represented adequately due to the adoption of the simple constitutive model Mohr-Coulomb. To investigate the behavior of the GRPS embankment, Houda *et al.* [17] performed several 3D small-scale model tests under low frequency cyclic load. The investigation revealed a settlement accumulation, particularly in the first ten cycles, where 50 % settlement accumulation occurred. Furthermore, applying the cycles increases load efficiency. After 20–30 cycles, a value of roughly 1, in which practically the full load is transferred to the pile heads, is obtained and thereafter remains stable.

Zhuang *et al.* [18] investigated a range of 3D finite element (FE) models of GRPS embankment under cyclic load. The parametric study revealed that settlements increase with vehicle wheel load and speed, whereas the soil arching is reduced

with larger vehicle load and speed. 3D numerical simulations of GRPS embankment were conducted in the Pham et al. [19] study. The analysis results indicated that the SCR decreases with the number of cycles due to the reduction of the soil arching, the vehicle speed contributes to quick dissipation of the soil arching. Additionally, the cumulative settlements increase as the vehicle speed and embankment height rise. The researchers also discovered that the influence of the number of geosynthetic layers could be negligible. Wang et al. [20] observed through the 3D dynamic analysis that the pile stiffness and the fixed end piles can reduce the stresses in the soft subsoil. Aqoub et al. [21], based on experimental analysis, observed an improvement of the GRPS embankment behavior related to the load efficiency and settlement under cyclic loading with the increase of geosynthetic layer numbers. It was noticeable that approximately 50% of the embankment surface settlement occurred during the first 100 cycles. On the other hand, the researchers found also that the geosynthetic tension increases during different cyclic loading stages, however, remains nearly constant in every stage.

The static and dynamic performance of GRPS embankment was investigated Bi et al. [22] numerically, the researchers observed that the SCR decreases under long-term traffic loads and the stiffness of the soft soil has a main role in undermining the performance of soil arching. They observed also that the differential settlements increase with the cycles number to finally be in a stable state. Zhuang et al. [23] evaluated the GRPS embankment under cyclic loading and unloading through the FE analysis. The parametric study demonstrates that the higher vehicle speed and the wheel load and the lower the geosynthetic stiffness, the load efficiency lower. Patel et al. [24] analyzed the dynamic response of GRPS embankment and found that for an embankment height to pile spacing ratio (a) of less than or equal to 4.5, geosynthetic stiffness of 3000 kN/m is adequate to achieve high SCR, as well as to decrease the differential settlements under dynamic loads and different heights of the embankment. If a is more than 4.5 then the SDR increases with the geosynthetic stiffness. Fang et al. [25] provided a dual-beam model to simulate the pavement and geosynthetic in order to assess the dynamic behavior of the GRPS embankment. The findings indicate that the moving load position has an influence on the GRPS embankment's stress and deflection distribution. Deflection and stress increase as the speed of the moving load increases. By increasing pile stiffness and geosynthetic modulus, the effect of moving load speed on the GRPS embankment can be decreased, these two parameters contribute to improve the stability of the GRPS embankments. Duan et al. [26] discussed the redistribution of the dynamic stress under moving train load due to the soil arching phenomenon in the embankment body and the contribution of geogrid in this process. 3D simulations are employed in the study to better elucidate the dynamics of GRPS embankments under a single cycle of high-speed train. Proper constitutive models are utilised to simulate the behavior of the bearing soil, soft soil and embankment fill based on the recommendations of Shahraki et al. [27] to better representation of their behavior. Results highlight the influence of using piles and the geosynthetic reinforcements to sustain the

embankment, and the behavior of the vertical stresses and settlements in the embankment body. The indices of describe the behavior of the GRPS embankment are different as shown in the literature, this paper adopts the load efficiency, the geosynthetic tension, and the settlements to find out the influences of the embankment height, cover ratio, and train speed on the aforesaid indices.

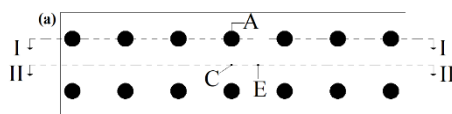
2 Finite Element Modelling

2.1 Description of GRPS Embankment Model

The technology employed to support embankments consists of (i) a network of vertical elements (piles), which are commonly slender and cylindrical in shape. The installation method (driving, boring, etc...) and mesh pattern (square, triangle, rectangle, etc...) of the piles are adopted based on soil conditions and both geometry and nature of applied loads. The installation of piles is regarded as the first stage of construction. (ii) a load transfer platform (LTP), this platform typically composed of a granular soil and one horizontal layer or more of geosynthetic reinforcement, and this is the second stage of construction. The last stage is the construction of the embankment body [28].

GRPS embankment is constructed atop a simple geological profile consisting of a 10-m soft soil layer resting on a stiff soil of gravel. The groundwater level is located directly at the soft soil layer surface. The 13.0 m wide embankment with a height of 2.6 m and slope angle of 1:1.15 is supported by a network of piles and one layer of geogrid as illustrated in Figure.1.

At the top of the embankment, a clustered ballast layer with a thickness of 0.35 m capped by transverse sleepers to support the railway track. In a square pattern, circular-cross-section piles with a diameter of 0.6 m and pile spacing of 2.0 m are installed. This network of piles penetrates the gravel's stiff layer. The geogrid layer with a stiffness of 5000 kN/m is located 0.1 m above the pile heads. The following points are utilized to display the outputs of the numerical analysis. Points B and D are located on the ballast surface. Points A, C, and E are located on the embankment's base level, as indicated in Figure 1. Longitudinally, Points D, C, and E are 2 meters from the boundaries, whereas Points B and A are 3 meters away.



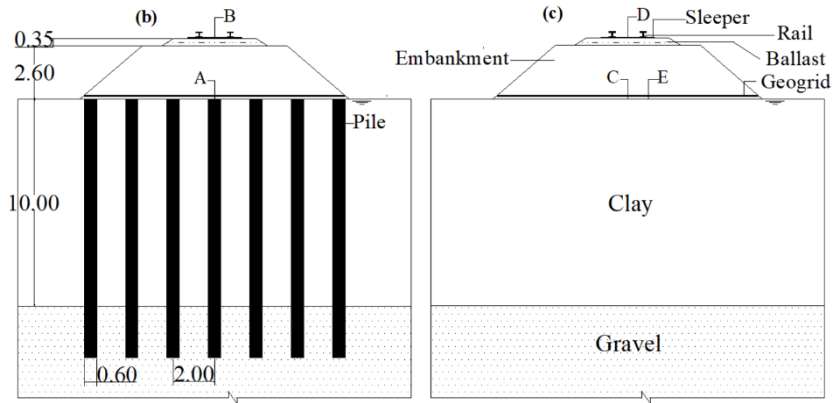
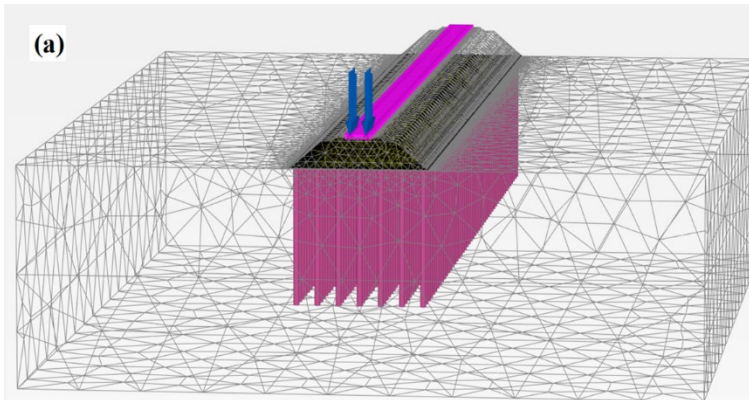


Figure 1

GRPS embankment profile (a) Plan view at the embankment base plane; (b) section I-I; (c) section II-II

2.2 3D Modelling of the Problem

To simulate the dynamic behavior of the GRPS embankment under the moving load which represents the high-speed train, a model of 96 m length and 45 m width was created in Plaxis 3D CONNECT Edition V20 program. The absorbent boundaries and Standard fixities were employed to minimize the reflections of the waves at the boundaries. The finite element mesh of the GRPS embankment is shown in Figure 2.



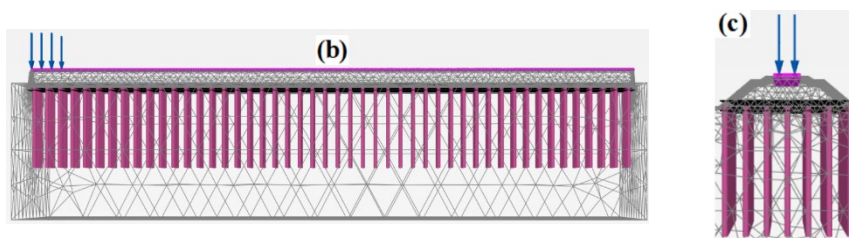


Figure 2

(a) Numerical model of GRPS embankment; (b) Side view; (c) Front view

The rails, rail fastening systems, and sleepers, all of which lay on the ballast layer and the underlying subgrade represent the typical components of the railway track [29]. The rails and sleepers are modeled as beam elements. The properties of UIC 60 rail [30] are adopted in the simulation, and the distance between the two rails is 1.5 m. The properties of concrete sleeper type B70 [30] are adopted by supplying the area moment of inertia, the model included 121 sleepers with a center-to-center distance of 60 cm. The properties of rail and sleepers are listed in Table 1.

Table 1
The properties of UIC60 rail and B70 sleeper

Basic parameters	Characters and units	UIC60 rail	B70 sleeper
Cross-sectional area	a (m ³)	0,0077	0.0513
Unit weight	γ (kN/m ³)	78	25
Young's modulus	E (MPa)	200000	36000
Inertia moments	I2 (m ⁴)	0,00000513	0.00024
	I3 (m ⁴)	0,00003	0.0253

The LM71 Eurocode load model was used to simulate the moving train, which includes eight dynamic point loads of 125 kN vertical force with a constant distance of 1.6 m. Each point load has its own dynamic multiplier in Plaxis 3D, which is characterized as a time-shear force signal. The “Beams on the elastic foundation” theory can be used to determine the shear forces in the rails. The shear force signal is multiplied by the dynamic point load (125 kN) in each time step, if the moving train's acceleration is negligible and the distance between the dynamic point loads is constant, the time step is deemed constant. In our case study, the train with speed of 250 km/h passes 1.6 m in 0.023 sec., the time frame during which the dynamic load may be deemed fixed is represented by the earlier period. In this model of 96 m long, the total time between the first and the last load is 1.38 sec., an extra 1.12 sec. was provided to dissipate the majority of the waves created by the moving train to obtain full dynamic time of 2.5 sec. All of the point loads have their values for each time step. As a result, the point loads are continually triggered and reach their maximum levels when the moving train passes over them.

2.2.1 Material Parameters

Benz [31] proposed the generalized Hardening Soil model with Small-strain stiffness (HSS) through the development of the Hardening Soil (HS) model, this model takes the small strain characteristics of soil at high stiffness into consideration. The HSS model exhibits typical hysteretic behavior under cyclic loading. Based on that, this model is used to simulate the behavior of embankment soil, soft soil, and the bearing layer soil [27]. Several authors have utilized the HSS model to simulate the soil behavior under dynamic loading in different geosynthetic reinforced earth (GRE) structures. They found that the results are consistent with the field measurements [32]. The ballast is modeled with Mohr–Coulomb (MC) model [27]. The properties of the different soils are listed in Tables 2 and 3.

The piles are represented by embedded beam elements with a unit weight of 24 kN/m³, a Young's Modulus of 20 GPa, and a Poisson's ratio of 0.20. The biaxial geogrid, on the other hand, is represented as an elastoplastic material.

Table 2
The properties of embankment fill, soft soil, and gravel

Basic parameters	Embankment fill	Soft soil	Gravel
Saturated unit weight: γ_{sat} (kN/m ³)	20.0	15.0	20.0
Unsaturated unit weight: γ_{unsat} (kN/m ³)	18.0	12.0	19.0
Internal friction angle: ϕ (°)	35.0	25.0	38.0
Dilatancy angle: Ψ (°)	5.0	0.0	8.0
Cohesion: c (kPa)	5.0	5.0	1.0
Reference secant stiffness: E_{50}^{ref} (kN/m ²)	36000	1500	48000
Reference tangent stiffness: E_{tend}^{ref} (kN/m ²)	36000	750	48000
Reference unloading /reloading stiffness: E_{ur}^{ref} (kN/m ²)	108000	6000	144000
Exponential power: m (-)	0.5	0.7	0.5
Reference shear modulus at small strain: G_0^{ref} (kN/m ²)	100800	15000	114400
Reference strain threshold: $\gamma_{0.7}$	0,00014	0.00026	0.00012
Coefficient of earth pressure at rest: K_0^{nc} (-)	0.419	0.5775	0.384
Unloading/reloading Poisson's ratio: ν_{ur} (-)	0.2	0.2	0.2

Failure ratio: R_f (-)	0.9	0.9	0.9
Permeability: k (m/day)	1.0	5.55E-4	1.00

Table 3
The properties of ballast soil

Ballast	$\gamma_{sat} = \gamma_{unsat} = 25$ kN/m ³	$\phi = 40^\circ$	$\Psi = 0^\circ$	$c = 10$ kPa
	$E = 100000$ kPa	$\nu = 0.2$	$k = 1.0$ m/day	

3 Results and Discussion

The reference case is created in order to investigate the behavior of the GRPS embankment under a single cycle of high-speed train. It is composed of a 2.6 m embankment supported by a network of piles and one layer of geogrid as indicated previously in section (2.1). A loading cycle is produced by a train speed of 250 km/h.

The first part of this study introduces the following:

- A comparison between the GRPS embankment and the conventional embankment with the behavior of settlements.
- A comparison of the behavior of vertical stresses and settlements under the static (embankment weight) and dynamic loads.
- The behavior of vertical wave velocity at two points (C, D).

A parametric analysis is conducted in the second part to examine the effect of the height of the embankment, cover ratio, and train speed on the behavior of the GRPS embankment in terms of the load efficiency (point A), the geosynthetic tension (point E), and the settlements at the ballast surface, (points D and B). The parametric analysis focuses on the time of the train operation. This time changes with the variation of the embankment height and moving train speed. For example, for different speeds ($v_1 = 80$ km/h, $v_2 = 160$ km/h, $v_3 = 250$ km/h), Plaxis 3D outputs demonstrate different time of the maximum load over the pile head ($t_1 = 0.36$ sec., $t_2 = 0.23$ sec., $t_3 = 0.16$ sec.) respectively.

3.1 Assessment of the Pile and Geogrid Influence on an Embankment Subjected to Moving Train Load

The embankment supported by a network of piles and one layer of geogrid was compared to the case of the unsupported (conventional) embankment to assess the function of the pile and geogrid in the dynamic response of the embankment erected over soft soil. Figure 3 depicts the embankment failure scenarios of the

entire geometry in two cases (A) unsupported embankment and (B) GRPS embankment.

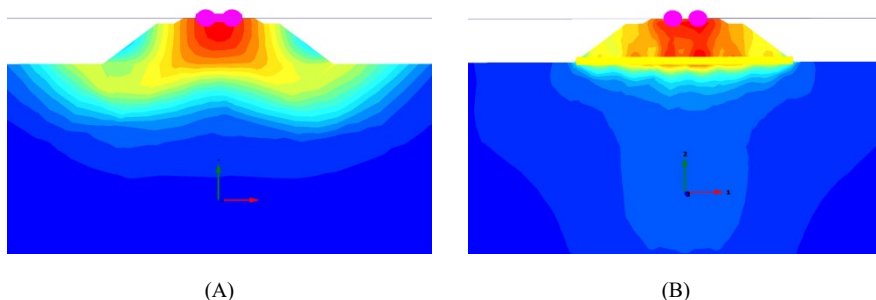


Figure 3

Failure scenario of (a) unsupported embankment, (b) GRPS embankment

For a more explanation, the piles serve to transfer the majority of the load to the bearing soil layer, reducing the load on the soft soil and, as a result, the vertical settlements of the railway structure. Furthermore, the geogrid reinforcement contributes to strengthen the embankment by increasing compressive strength, which reduces the effect of dynamic loads on the railway structure. Figure 4 shows the maximum vertical settlement behavior at the ballast surface (point D) in the two scenarios during the train's passage ($t=0.16$ sec.). The use of piles and geogrid aids in reducing the vertical settlement to a reasonable level.

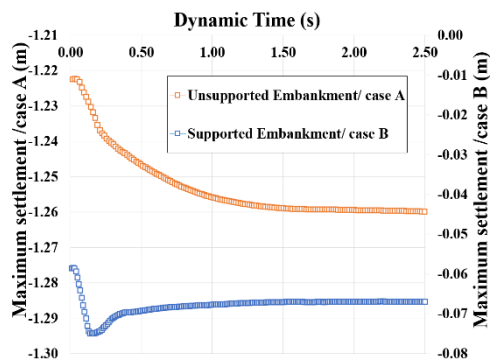


Figure 4

Vertical settlements of (a) unsupported embankment, (b) GRPS embankment

3.2 Stress Distribution in the GRPS Embankment

The stress distribution along the embankment body over the pile head (point A) and in the midway between four piles (point E) is investigated. The investigation was conducted under the static and dynamic loads.

At the ballast surface, the vertical stress over the pile axis equal to 0 kPa under static load, the amplitude of the vertical stress increases with the depth progressively to attain the maximum value over the pile head. Regarding the dynamic load, the vertical stress commences with 210 kPa owing the train load, this value reduces with depth before increasing again near the embankment base and attain the maximum value over the pile head as illustrated in Figure 5.

On the other side, the stress distribution behaves differently over the midpoint between the piles; the vertical stress increases to a specified depth, then starts to decrease due to the formation of the soil arch, and subsequently increases again to a small extent due to the weight of the soil under the arch. It is noteworthy that the vertical stress distribution under the static and dynamic loads is similar. As illustrated in Figure 5, the soil arch height in this reference case is 0.83 m, representing the phase of vertical stress reduction in the structure.

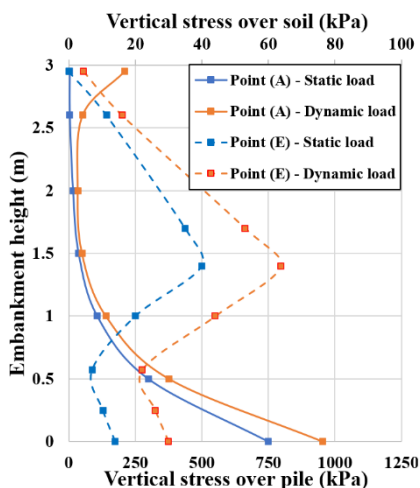


Figure 5

Vertical stress distributions in the GRPS embankment body

3.3 Vertical Settlement Distribution in the GRPS Embankment

The settlements as a function of the embankment height are illustrated in Figure 6 through points (B, D) on a vertical profile. The settlement distributions were investigated the static and dynamic loads.

The maximum settlements decrease with the depth over the pile and soil as illustrated in Figure 6. It is noticeable also that the differential settlements under the dynamic loading is larger than those under the static loading.

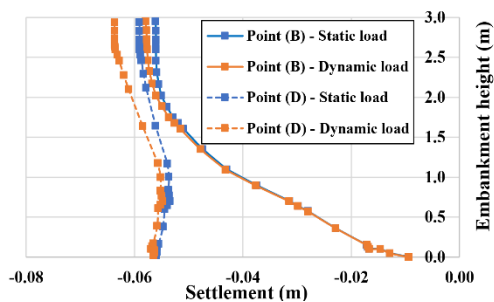


Figure 6

Vertical settlement distribution along the GRPS embankment height

The results show that the maximum value of the differential settlement between the points (B, D) is 0.0047 m. The intersection point of the two curves (oranges or blues) represents the critical height, in this reference case, the authors determined that the critical height is more than 2.95 m. The critical height represents the height from the pile head level to the plane of equal settlements in the embankment body. In other words, the differential settlements can be negligible over this plane.

3.4 Vertical Velocity in the GRPS Embankment

Figure 7 shows the vertical velocity at points (D, C). The peak of the observed amplitude at the ballast surface culminates during the train's passage. The vertical velocity begins to attenuates progressively after the train's passage, on the other hand, the amplitude of the vertical velocity decreases with the depth as illustrated in Figure 7. It is noticeable the low value of the velocity at point (C), this is attributed to the involvement of piles and geogrid in improving the ability of the soft soil to attenuate the velocity in this medium.

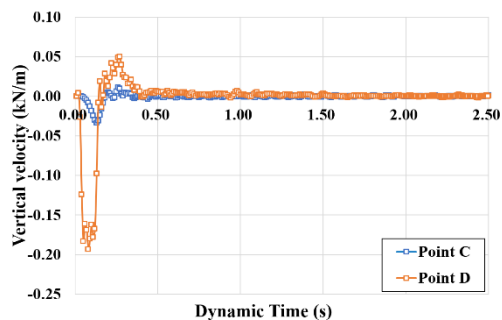


Figure 7

Vertical velocity of different depths

3.5 Parametric Study

3.5.1 Influence of GRPS Embankment Height (H)

To consider the influence of the embankment height, the applied load over the pile head and the load efficiency are investigated during the passage of the train. Figure 8 demonstrates that the applied load increases to a large extent under the dynamic loading before decreasing after the train passes. At the same time, despite receiving an additional load, it is clear that load efficiency reduces dramatically. This may be read as the inability of the soil arch to transfer a considerable portion of the dynamic load to the pile, which is reflected in more settlements of the soft soil. The load efficiency increases again under the pure load of the self-weight of the embankment.

Figure 8 further illustrates that the load efficiency increases with the higher embankment under static and dynamic loading. Moreover, the magnitude of the dynamic load transferred to the pile head increases as the embankment height decreases.

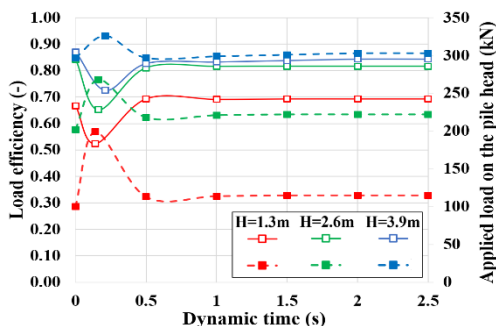


Figure 8

The load efficiency in the dynamic time for different embankment heights (Dashed curve represents the vertical load on the pile head, solid curve represents the load efficiency)

Figure 9 shows the geosynthetic tension for different embankment heights. As shown in the Figure, for a given dynamic time the geosynthetic tension increases when the height increases. It is obvious that the tension increases significantly for the low embankment ($H=1.3$ m) with a tendency to be constant progressively after the passage of train.

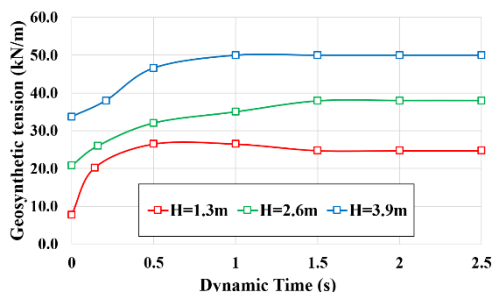


Figure 9

The tension in the geosynthetic for different embankment heights

Figure 10 illustrates the variance in maximum and differential settlements at point D and points (D, B) on the ballast surface respectively. Due to the increased self-weight of the embankment, the maximum vertical settlement (columns) of point D increases with the embankment height during the train passage. On the other side, the differential settlements (lines) decrease as the embankment height increases progressively as explained in section (3.3). As can be seen, the differential settlements for the different presumed embankment heights cannot be neglected.

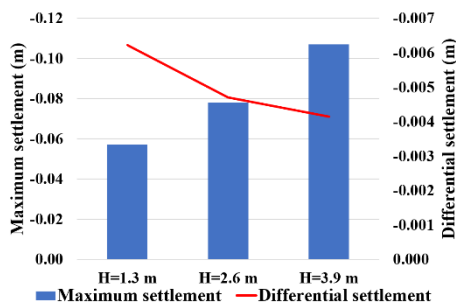


Figure 10

The maximum and differential settlements at the ballast surface for different embankment heights

3.5.2 Influence of Cover Ratio (a)

The effect of the cover ratio variation in the dynamic time domain has been investigated. For this purpose, three diameters of the pile are used (0.6 m, 0.8 m, 1.0 m). The cover ratio can be governed by adjusting the pile diameter or by enlarging the pile cap. In this reference case, the cover ratio is controlled by the pile diameter. The results are depicted in Figure 11. As can be noticed, increasing the cover ratio lower the load efficiency. The influence of the cover ratio is more noticeable under the static load than dynamic load.

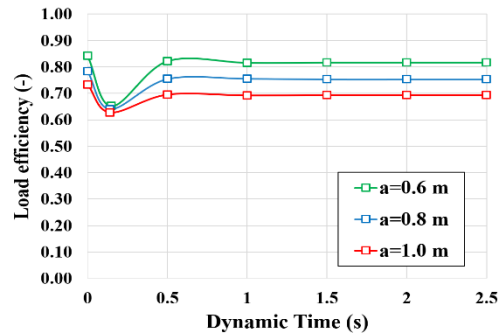


Figure 11

The load efficiency in the dynamic time for different cover ratios

This phenomenon can be explained as follows, with larger pile diameter, the pile's skin friction area expands. Consequently, the negative skin friction generated by the stresses over the soft soil along the upper part of the pile increases. Conversely, the load applied on the pile's head decreases. The axial forces distribution along the pile shaft is illustrated in Figure 12.

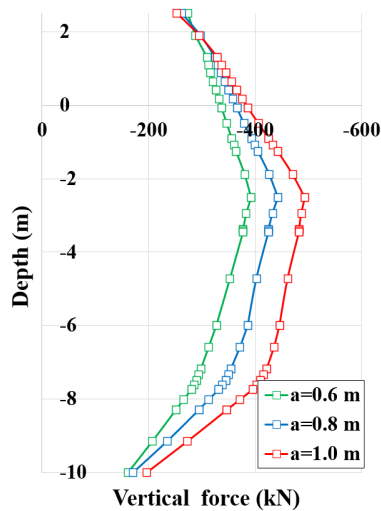


Figure 12

The axial forces distribution for different pile diameters

The utilize of large-diameter piles contributes to boost the stability of the soil arch; in consequence, the magnitude of load transfer through the soil arch improves while that transferred to the pile via geosynthetic reinforcement to the piles diminish.

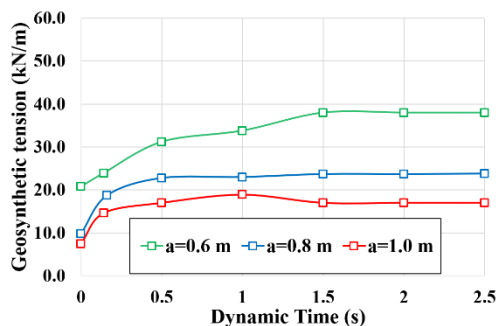


Figure 13

The tension in the geosynthetic for different cover ratios

Based on that, the increase of the cover ratio reduces the tension in the geosynthetic which in turn tends to be stable after the train passage as shown in Figure 13. It was noticeable in this study that the maximum tension in the geosynthetic occurs at the edge of the pile.

Figure 14 depicts the maximum and differential settlements at the ballast layer surface for various pile diameters. It can be seen that settlements decrease as the cover ratio increases. The reason for this is that the soil arch develops with the increased cross-sectional area of the pile, which contributes to restrict the amount of stress applied to the soft soil.

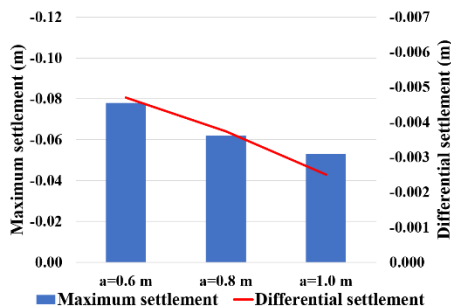


Figure 14

The maximum and differential settlements at the ballast surface for different cover ratios

3.5.3 Influence of Train Speed (v)

The influence of moving train speed on load efficiency is discussed in this section in which compares the findings of three different speeds, e.g. 80, 160, and 250 km/h at the corresponding times (t) = 0.36, 0.23, and 0.16 sec., respectively, as shown in Figure 15. The higher train speeds reduce the vertical stress transferred to the pile heads. This might be because the amplitude and frequency of the

dynamic load increased with speed [33]. These results are compatible with those of Pham *et al.* [19]. The researchers found that the SCR is closer to equal to 1.0 with high speeds after limited number of cycles, in other words, the soil arching reduction is faster with the higher speeds.

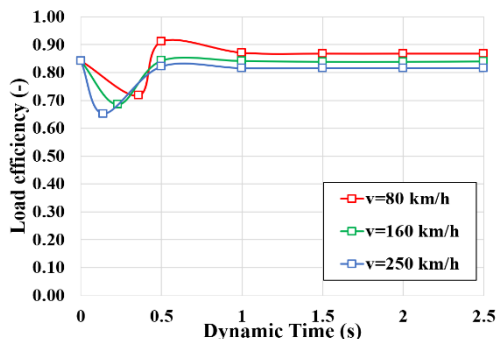


Figure 15

The load efficiency in the dynamic time for different train speeds

The use of a geogrid contributes to regulate the vibration in the soil during the train passage. Referring to the effect of the train speed on the geosynthetic tension. Figure 16 shows that the geosynthetic tension of 80 km/h speed is the highest under the dynamic loading. Conversely, it is noticeable that the tension increases with speed at the end of the dynamic time (static loading). The Figure 16 shows also that the different behavior of the geosynthetic tension with the various speeds.

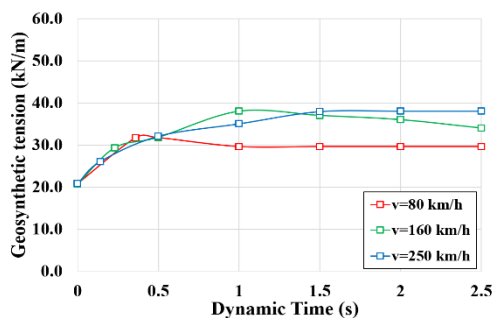


Figure 16

The tension in the geosynthetic for different train speeds

Figure 17 refers to the effect of the train speeds on the maximum and differential settlements. It is visible from the preceding results that the load efficiency reduces with speed, and as a consequence, the vertical stresses applied to soft soil rise. Figure 17 depicts the development of the settlements at the ballast surface; the maximum settlements increase with the high speeds. At the same time, the differential settlements decrease as demonstrated by Meena *et al.* [34].

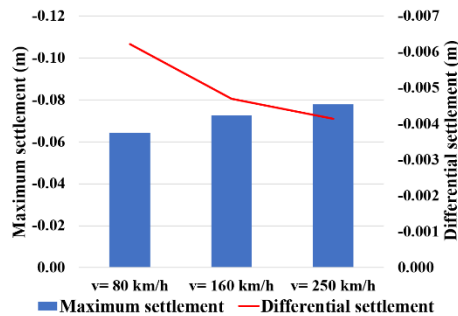


Figure 17

The maximum and differential settlements at the ballast surface for different train speeds

Conclusions

In this study, the authors used 3D numerical method to investigate the behavior of a GRPS embankment during a single high-speed train cycle. To simulate the behavior of bearing soil, soft soil, and embankment fill, the Hardening soil model with small-strain stiffness was utilized. The dynamic load which represents the moving train was modeled using the LM71 Eurocode recommendations. The following conclusions are obtained:

- The piles and geogrid reinforcement contribute significantly to support the railway track through the reduction of the vertical settlements to a reasonable level.
- The distribution of the vertical stresses in the embankment body is similar under the static and dynamic loading. So is the case for the distribution of the vertical settlements.
- The vertical velocity of the waves decreases with the depth remarkably due to the involvement of piles and geogrid in improving the ability of the soft soil to attenuate this velocity.
- The magnitude of the dynamic load transferred to the pile head decreases as the embankment height increases. An increase in the embankment height results in an increase in the load efficiency and the maximum settlement and a decrease in the differential settlement at the ballast surface.
- The increase of the cover ratio by the cross-sectional area of the pile lower the load efficiency due to the increase of the negative skin friction generated by the stresses over the soft soil along the upper part of the pile. The higher cover ratios improve the stability of the railway track due to the reduction of the maximum and differential settlements.
- Given the different train speeds, the higher train speeds reduce the load efficiency, and as a consequence, the maximum settlements increase at the ballast surface. While the results related to the differential settlements indicate that these settlements decrease with the faster the train speeds.

References

- [1] Sz. Fischer, Investigation of the Horizontal Track Geometry regarding Geogrid Reinforcement under Ballast, *Acta Polytechnica Hungarica*, Vol. 19, No. 3, 2022, pp. 89-101
- [2] L. Briançon, B. Simon, Pile-supported embankment over soft soil for a high-speed line, *Geosynthetics International*, Vol. 24, No. 3, 2017, pp. 293-305
- [3] P. Ariyaratne, D. S. Liyanapathirana, Review of existing design methods for geosynthetic-reinforced pile-supported embankments, *Soils and Foundations*, Vol. 55, No. 1, 2015, pp. 17-34
- [4] K. Terzaghi, *Theoretical soil mechanics*, Soils and Foundations, 1943, New York: John Wiley and Sons
- [5] B. Low, S. Tang, Arching in piled embankments, *Journal of Geotechnical Engineering*, Vol. 120, No. 11, 1994, pp. 1917-1938
- [6] D. Russell, N. Pierpoint, An assessment of design methods for piled embankments, *Ground Engineering*, Vol. 30, No. 11, 1997, pp. 39-44
- [7] S. Abusharar, J. Zheng, B. Chen, J. Yin, A simplified method for analysis of a piled embankment reinforced with geosynthetics, *Geotextiles and Geomembranes*, Vol. 27, No. 1, 2008, pp. 39-52
- [8] BS8006, *Code of Practice for Strengthened Reinforced Soils and Other Fills*, London, UK, 2010
- [9] EBGeo, *Recommendations for design and analysis of earth structures using Geosynthetic Reinforcements*, German geotechnical society, 2011
- [10] Dutch standard CUR226, *Design guideline basal reinforced piled embankments*, CRC press, 2016
- [11] T. Pham, Analysis of geosynthetic-reinforced pile-supported embankment with soil-structure interaction models, *Computers and Geotechnics*, Vol. 121, 2020, pp. 1-17
- [12] C. Heitz, J. Lüking, H. G. Kempfert, *Geosynthetic Reinforced and Pile supported Embankments under Static and Cyclic Loading*, 4th European Geosynthetics Conference, Edinburgh, UK, 2008
- [13] C. Yu, L. Pan, B. Qian, J. Cai, *The Behavior of Piled Embankments under Embankment Loads and Traffic Loads*, Second International Conference on Transportation Engineering, 2009, Chengdu, China, pp. 1566-1571
- [14] J. Han, A. Bhandari, *Evaluation of Geogrid-Reinforced Pile-Supported Embankments under Cyclic Loading using Discrete Element Method*, Proceedings of the US-China Workshop on Ground Improvement Technologies, 2009, Orlando, Florida, United States, pp. 73-82

- [15] G. Han, Q. Gong, S. Zhou, Soil Arching in a Piled Embankment under Dynamic Load, *International Journal of Geomechanics*, Vol. 15, No. 6, 2015, pp. 04014094-1 to 7
- [16] Y. Zhuang, S. Li, Three-dimensional finite element analysis of arching in a piled embankment under traffic loading, *Arabian Journal of Geosciences*, Vol. 8, No. 10, 2015, pp. 7751-7762
- [17] M. Houda, O. Jenck, F. Emeriault, Physical evidence of the effect of vertical cyclic loading on soil improvement by rigid piles: a small-scale laboratory experiment using Digital Image Correlation, *Acta Geotechnica*, Vol. 11, No. 2, 2016, pp. 325-346
- [18] Y. Zhuang, K. Wang, Finite element analysis on the dynamic behavior of soil arching effect in piled embankment, *Transportation Geotechnics*, Vol. 14, 2018, pp. 8-21
- [19] H. V. Pham, D. Dias, A. Dudchenko, 3D modeling of geosynthetic-reinforced pile-supported embankment under cyclic loading, *Geosynthetics International*, Vol. 27, No. 2, 2018, pp. 8-21
- [20] D. Wang, M. Sanchez, J. L. Briaud, Numerical study on the effect of rigid inclusions on existing railroads, *Int J Numer Anal Methods Geomech*, Vol. 43, No. 18, 2019, pp. 2772-2796
- [21] K. Aqoub, M. Mohamed, T. Sheehan, Analysis of unreinforced and reinforced shallow piled embankments under cyclic loading, *Geosynthetics International*, Vol. 27, No. 2, 2019, pp. 182-199
- [22] Z. Bi, Q. Gong, J. Huang, Long-Term Stability of High-Speed Railway Geosynthetic Reinforced Pile-Supported Embankment Subjected to Traffic Loading Considering Arching Effect, *Transportation Research Board*, Vol. 2674, No. 7, 2020, pp. 596-607
- [23] Y. Zhuang, X. Cui, S. Zhang, G. Dai, X. Zhao, The load transfer mechanism in reinforced piled embankment under cyclic loading and unloading, *European Journal of Environmental and Civil Engineering*, Vol. 26, No. 4, 2020, pp. 1364-1378
- [24] R. M. Patel, B. R. Jayalekshmi, R. Shivashankar, Stress Distribution in Basal Geogrid Reinforced Pile-Supported Embankments Under Seismic Loads, *Transportation Infrastructure Geotechnology*, Vol. 8, No. 3, 2021, pp. 516-541
- [25] H. Fang, J. J. Zheng, Y. Liu, R. Y. Hou, Z. R. Jia, Analytical solutions of the dynamic response of a dual-beam model for a geosynthetic reinforced pile-supported embankment under moving load, *Computers and Geotechnics*, Vol. 142, 2022

-
- [26] X. Duan, Y. Wu, X. Bian, J. Jiang, Dynamic Behaviors of Piled Embankment Under High-Speed Train Loads, *Advances in Transportation Geotechnics IV*, Vol. 166, 2022, pp. 1041-1047
- [27] M. Shahraiki, M. Sadaghiani, K. J. Witt, Th. Meier, 3D Modelling of Train Induced Moving Loads on an Embankment, *Plaxis Bulletin*, Autumn issue, 2014, pp. 10-15
- [28] R. Alsirawan, Review of Geosynthetic-Reinforced Pile-Supported (GRPS) embankments- parametric study and design methods, *Acta Technica Jaurinensis*, Vol. 14, No. 1, 2021, pp. 36-59
- [29] Sz. Fischer, Geogrid reinforcement of ballasted railway superstructure for stabilization of the railway track geometry – A case study, *Geotextiles and Geomembranes*, In press, 2022
- [30] E. Koch, Finite element analysis of bridge transition zone for investigating the effect of moving loads. 17th European Conference on Soil Mechanics and Geotechnical Engineering, Reykjavik, Iceland, 2022
- [31] T. Benz, Small-strain stiffness of soils and its numerical consequences, PhD Thesis, 2007, University of Stuttgart
- [32] A. Herold, P. A. Von Wolfersdorff, The Use of Hardening Soil Model with Small-Strain Stiffness for Serviceability Limit State Analyses of GRE Structures, *Proceedings of GeoAfrica 1*, 2009, Cape Town, South Africa
- [33] Y. M. Zhang, B. Liang, Dynamic response of expressway subgrade under geometric irregularity conditions, *Journal of Lanzhou Railway University*, Vol. 20, No. 4, 2001, pp. 66-69
- [34] N. K. Meena, S. Nimbalkar, B. Fatahi, G. Yang, Effects of soil arching on behavior of pile-supported railway embankment:2D FEM approach, *Computers and Geotechnics*, Vol. 123, 2020